Precursor signatures and evolution of post-sunset equatorial spread-F observed over Sanya

Guozhu Li,[1] Baiqi Ning,[1] M. A. Abdu,[2] Weixing Wan,[1] and Lianhuan Hu[1]

Received 9 April 2012; revised 4 July 2012; accepted 5 July 2012; published 21 August 2012.

[1] Recent case studies on the precursor signatures of equatorial spread-F (ESF) have shown a one-to-one correspondence between the large-scale wave structures (LSWS) and ESF development at equatorial latitude. In this study, the LSWS and the onset and development of the ESF are investigated over Sanya (18°N, 109°E), a station located at 13° north of the magnetic equator, during both geomagnetic quiet and disturbed conditions in September–October 2011. High-time-resolution ionograms from Digisonde Portable Sounder (DPS-4D) provided the satellite trace measurements that were used to indicate the occurrence of the LSWS. The development of local ESF activity was identified using GPS scintillation and VHF coherent radar echo measurements from the same site, together with the range type spread-F (RSF) in ionograms. Additionally, the Sanya VHF radar five-beam scanning measurements in east–west direction were used to characterize the longitudinal difference in establishing the initial conditions for ESF development. Correlative studies between the LSWS and ESF activities during the observational period offer consolidated evidence that the LSWS is a necessary precursor for the ESF development. It is shown that the LSWS and ESF have nearly a one-to-one relationship when the F layer undergoes an abrupt post-sunset rise (PSSR), revealing that the magnitude of the pre-reversal enhancement in zonal electric field (PRE) that elevates the F layer to a high enough altitude is an important parameter controlling the generation of post-sunset ESF. However, in the absence of the PSSR, the ESF and GPS scintillation did not always occur following the appearance of LSWS. Sometimes the LSWS events preceded the generation of bottom type spread-F (BSF) that did not develop vertically into ESF and radar plumes. This result may indicate that under inexpressive, weak, or even moderate PRE conditions, the appearance of the LSWS alone may not be sufficient to produce the post-sunset F region irregularities responsible for ionospheric scintillations. More factors, other than the LSWS, could play crucial roles favoring the growth of ESF instabilities responsible for ionospheric scintillations.

Citation: Li, G., B. Ning, M. A. Abdu, W. Wan, and L. Hu (2012), Precursor signatures and evolution of post-sunset equatorial spread-F observed over Sanya, *J. Geophys. Res.*, *117*, A08321, doi:10.1029/2012JA017820.

1. Introduction

[2] The F region plasma irregularities with scale sizes from meters to hundreds of kilometers in the equatorial ionosphere are commonly referred to as the equatorial spread-F (ESF), which produce ionospheric scintillations that often profoundly impact satellite communication and navigation systems. Many aspects of the ESF, such as its occurrence statistics, longitudinal and seasonal distribution, and the dependence on solar and magnetic activity, have been reasonably well studied using ground based and in situ satellite borne measurements, and theoretical model simulations [e.g., *Kil and Heelis*, 1998; *Fejer et al.*, 1999; *Huba et al.*, 2008; *Retterer*, 2010]. From these investigations it is known that most ESF, which is often initiated in the post-sunset hours, are controlled mainly by a few factors, including the pre-reversal enhancement in zonal electric field (PRE), the seed perturbations, the density gradient at the bottomside of the F layer and the meridional/transequatorial winds [e.g., *Abdu*, 2001]. Under the action of the PRE, the ionosphere is rapidly elevated to higher altitudes with a steep plasma density gradient in the bottomside of the F region, favoring the growth of the irregularities by the Rayleigh-Taylor instability mechanism. It has been established that the PRE, in a climatological sense, for instance, in the global longitudinal and seasonal variation, is the most important parameter controlling the generation of ESF at solar maximum [e.g., *Abdu et al.*, 1983; *Fejer et al.*, 1999; *Li et al.*, 2007; *Chapagain*

[1]Beijing National Observatory of Space Environment, Institute of Geology and Geophysics, Chinese Academy of Sciences, Beijing, China.
[2]Divisão de Aeronomia, Instituto Nacional de Pesquisas Espaciais, São Paulo, Brazil.

Corresponding author: G. Li, Beijing National Observatory of Space Environment, Institute of Geology and Geophysics, Chinese Academy of Sciences, Beijing 100029, China. (guozlee@hotmail.com)

0148-0227/12/2012JA017820

et al., 2009, and references therein]. However, from the viewpoint of day-to-day variability needed for specifications of the irregularity effects in space based operational systems, the ESF appears to be related also to additional important factors other than the PRE [e.g., *Hysell and Burcham*, 2002; *Tsunoda*, 2005]. During seasons of high occurrence probability for the ESF at a given location, the ESF might be absent on some nights, even when the strength of PRE is similar to that on an ESF night.

[3] In attempts to understand the day-to-day variability in ESF, studies in recent years have revealed the role of seeding perturbation as a dominant source of such variability. Using the ALTAIR radar observations over Kwajalein Atoll, *Tsunoda* [2005] found that the ESF tended to be more closely related to the occurrence of large-scale wave structure (LSWS) that developed in the bottom side F layer than to the strength of PRE. More recent case studies from coherent scatter radar multibeam steering measurements, and low inclination satellite to ground TEC observations, have shown that LSWS always preceded the appearance of ESF [e.g., *Tsunoda and Ecklund*, 2007; *Thampi et al.*, 2009]. There appears to be a consensus now that the LSWS is a reliable precursor of ESF occurrence. The LSWS generation is attributed, in part, to the collisional shear instability [*Hysell and Kudeki*, 2004] that is driven by a velocity shear in the presence of a density gradient near sunset, and the large-scale polarization electric field that is generated by gravity waves or a sporadic E layer instability and mapped to the bottomside of the F layer along geomagnetic field lines [e.g., *Tsunoda*, 2006; *Abdu et al.*, 2009a; *Takahashi et al.*, 2009]. Due to the reason that the LSWS grows in amplitude without significant zonal drift, it is not easily detectable from overhead measurements using a sensor at a fixed location, for example, a fixed beam radar which does not uniquely distinguish between a locally forming backscatter plumes from a plume that drifted from the west.

[4] Thus far, the direct measurements of the LSWS were made mostly by the steerable ALTAIR incoherent scatter radar and by the GNU radio beacon (GRB) receivers [e.g., *Tsunoda*, 2005; *Thampi et al.*, 2009]. Using the GRB receiver network in Southeast Asia and Pacific low latitude regions, *Tulasi Ram et al.* [2012] developed a method to derive the characteristics of zonal LSWS on a regular basis. On the other hand, *Abdu et al.* [1981] showed that satellite traces preceded range type spread-F (RSF) in the ionograms over an equatorial station Fortaleza. Further, using the COPEX campaign data set, *Abdu et al.* [2009b] found that satellite traces appeared nearly simultaneously at the magnetically conjugate low latitude sites Boa Vista and Campo Grande. Such satellite traces and multireflected echoes in ionograms have been identified as direct signatures of the LSWS [*Tsunoda*, 2008]. This means that ionosondes, those are widely distributed at equatorial and low latitudes, can be used to detect the appearance of the LSWS.

[5] Though many case studies have revealed a one-to-one correspondence between the LSWS and ESF, there is still no general consensus about the role of the LSWS on the occurrence of ESF. More recently, *Narayanan et al.* [2012] reported a case in which the LSWS appeared but without subsequent ESF development. In the present study, we discuss results related to the onset and development of the post-sunset ESF and the occurrence of LSWS during a high occurrence season (equinoctial months September–October) of ESF at Sanya (18°N, 109°E; Dip latitude 13°N). Several typical examples of the Sanya VHF radar multibeam steering measurements, including well-developed plumes that drifted from the western longitude of Sanya, freshly generated plumes within the scanned area and the absence of post-sunset plume, are analyzed. A GPS scintillation receiver and a Digisonde operated over Sanya have also provided a good data set, which sheds light on the interesting aspect of statistical dependence of the ESF on a precursor LSWS. The overall analysis focuses mainly on the following issues: 1) Can the LSWS be observed at a low latitude site like Sanya located in this longitude region? If so, is it a necessary precursor signature for ESF occurrence? 2) Is there a statistical one-to-one correspondence between the LSWS and ESF? Alternatively, does the ESF that produce ionospheric scintillation always occur in sequence to the LSWS observed around sunset during the ESF high occurrence season? Notably, the radar multibeam steering observations that complement this study are the first of its kind from Sanya and are expected to shed light on the characteristic of the LSWS in this longitude region.

2. Instrumentation

[6] The Sanya VHF coherent scatter radar, with an operating frequency of 47.5 MHz and a peak power of 24 kW, is sensitive to irregularities of 3-m scale size and is a useful tool to study the low-latitude E region, the valley and the F region irregularities [e.g., *Li et al.*, 2011]. Generally, the radar beam is pointed toward the north at a zenith angle of 23°. The antenna pattern, with a 3 dB beam width of 10° in East–west and 24° in North–south, satisfies the field line perpendicularity condition at both E and F region heights, and can detect the coherent backscatter echoes arising from the field aligned irregularities (FAIs). Also, the radar has a capability to steer the beam within ±45° in azimuth around north. In this study, the radar beam was switched (steered) among five directions with azimuth and zenith angles of (45°, 33°), (32°, 29°), (0°, 23°), (328°, 29°), and (315°, 33°) that covered directions from east to west, satisfying the radar beam-magnetic field line perpendicularity condition in the height regions of interest. The fixed beam and beam-steering measurements were conducted to obtain ESF occurrence on the nights of 1 September to 20 October 2011 and 21–30 October 2011, respectively. The basic radar parameters during the period are listed in Table 1.

[7] Ionospheric scintillation measurements were performed using the GPS Ionospheric Scintillation and TEC Monitor (GISTM) system GSV4004A operated at Sanya. The amplitude scintillation was monitored by computing the S_4 index defined as the standard deviation of the received signal power normalized to the average signal power. It is calculated for each 1-min period based on a 50-Hz sampling rate. The GISTM also computes the S_4 index due to ambient noise in such a way that a corrected S_4 index (without noise effects) can be computed. In this study, only the corrected S_4 values with elevation angles of GPS satellites greater than 30° and with lock time greater than 180 s were used to identify the scintillation occurrence. On the other hand, the co-located Digisonde Portable Sounder (DPS-4D) was

Table 1. The Sanya VHF Radar Parameters Used for ESF Measurements During September 1 to 30 October 2011

Parameter	Value
Location	18°N, 109°E, dip 13°N
Operating frequency	47.5 MHz
Antenna	2 × 12 five-element Yagi antennas aligned in East–west
Gain	22 dB
Beam width	10° in azimuth, 24° in zenith
Peak power	24 kW
Pulse repetition frequency (PRF)	160 Hz
Number of coherent integrations	4
Range coverage	80–800 km
Range resolution	4.8 km
Time resolution	1 min
Fixed beam mode (1 Sep to 20 Oct)	beam toward north (0°, 23°)
Beam steering mode (21–30 Oct)	beam from east to west (45°, 33°), (32°, 29°), (0°, 23°), (328°, 29°), (315°, 33°)

operated every 5 min to obtain an ionorgam on 1 September to 30 October 2011.

3. Results and Discussion

3.1. Cases of LSWS With Subsequent ESF Development

[8] Digisonde ionograms and radar echo measurements have been widely used to investigate the onset and development of ESF structures. During the observational period 1 September to 30 October 2011, many ESF events were detected by the GPS scintillation receiver, the Digisonde and the VHF radar over Sanya. As an example, Figures 1 and 2 show, respectively, the spread-F initiation sequence in ionograms, and the spatial structure and temporal variation of backscatter echoes observed by the radar on the evenings of 24 and 26 October 2011. The spread-F usually begins with the appearance of satellite traces (indicated by arrows) adjacent to the main F layer trace in ionograms, suggesting the presence of large-scale wave structures (LSWS) in the bottomside electron density distribution. For the event of 24 October, Figure 1 (top) shows a satellite trace that first appeared in the ionogram at 1140 UT (UT = LT − 7.5 h). As inferred from the color scale (representing echoes arrived from different directions), the trace corresponds to an echo source located east of the station. The range separation between the satellite trace and the main F layer trace is about 25 km. Another ionogram taken 10 min later at 1150 UT displays more satellite traces, located both east and west of the station. The range difference between the main and multiple satellite traces varied between 25 and 100 km. After about 15 min, range type spread-F (RSF) appeared in the ionogram taken at 1205 UT. It is found that the satellite traces (appearing above or below the main F layer) coexisted with the RSF until 1300 UT (the second hop traces at this time are due to the tilted layer structure). The time between the first appearances of satellite traces and RSF is 25 min.

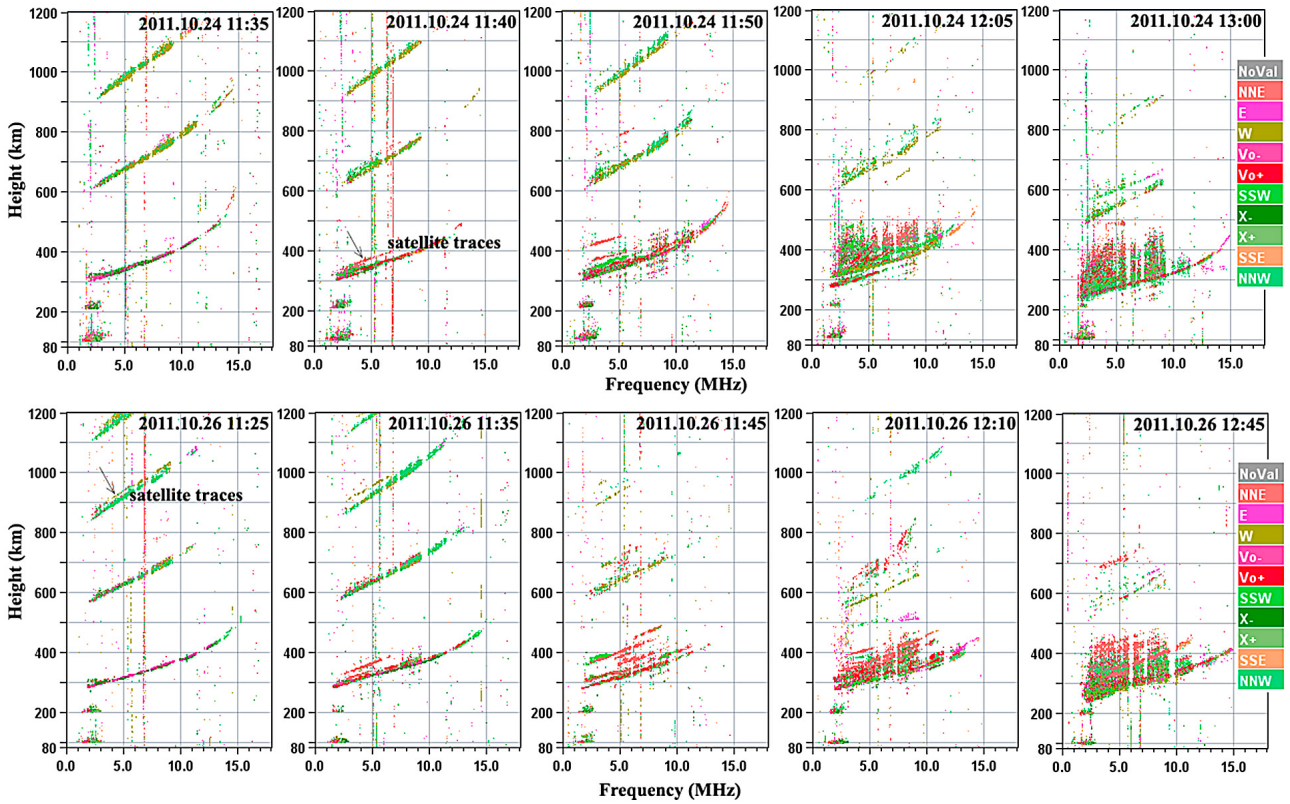

Figure 1. Sequential ionograms on (top) 24 and (bottom) 26 October 2011 over Sanya. The arrows show the appearance of off-vertical traces (satellite traces) close to the main or multihop F traces, indicative of the appearance of large-scale wave structures (LSWS).

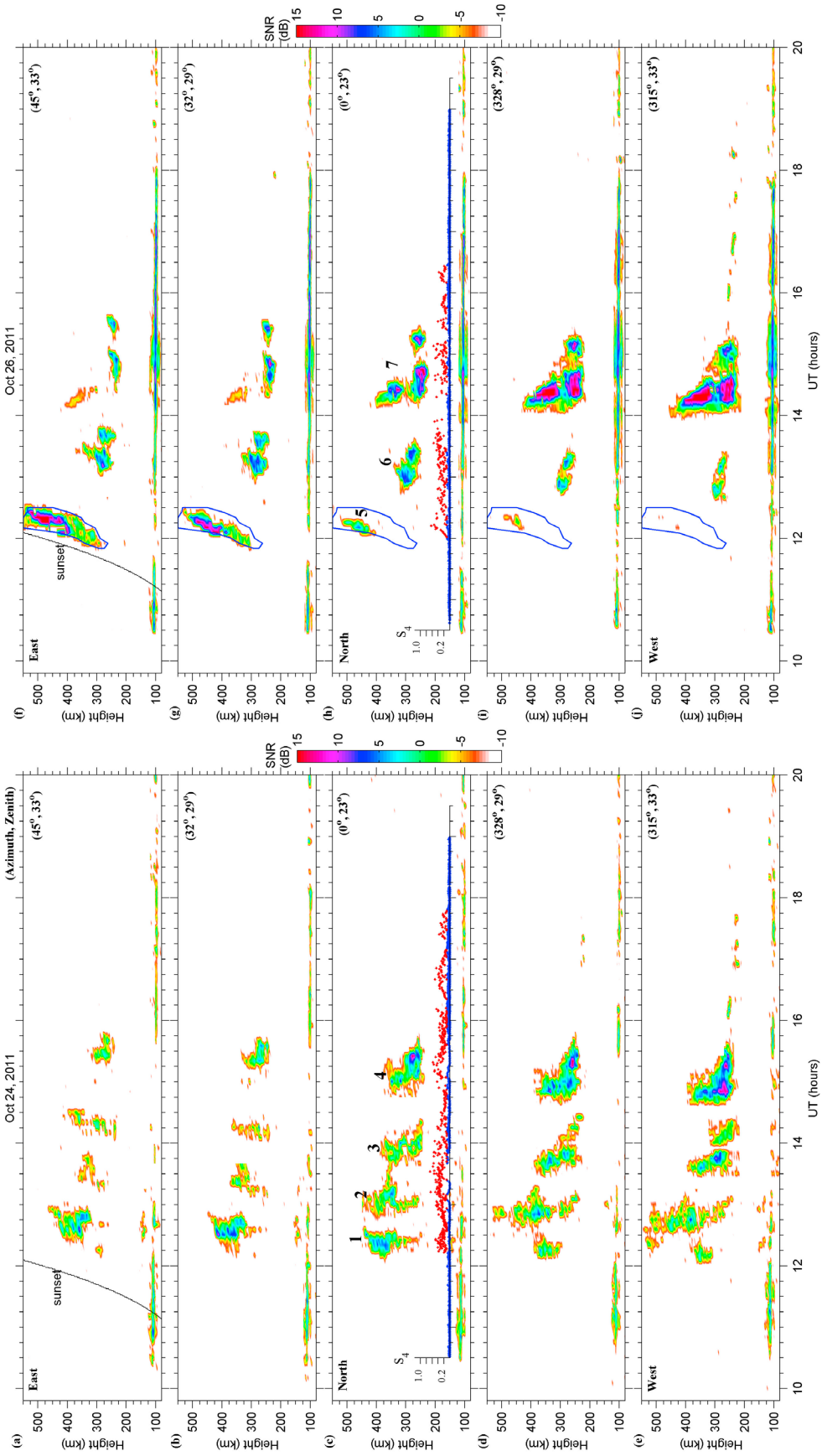

Figure 2. Range-time-intensity (RTI) maps of backscatter echoes obtained from the Sanya VHF radar five-beam steering measurement on (a–e) 24 and (f–j) 26 October 2011. The slant black lines indicate the sunset terminator over Sanya. The variations in the GPS scintillation index S_4 are plotted in red (for $S_4 > 0.1$) in Figures 2c and 2h wherein the periodic plume structures are labeled by numbers 1 to 7. The closed blue curve in Figures 2f–2j highlights the height-time interval of plume 5 which is dominant in the easternmost beam.

Table 2. Statistics for the Periodically Spaced Plume Structures During 21–30 October 2011

Events	Number of Plumes	Zonal Drifts[a] (Eastward, m/s)	Time Intervals (min)	Zonal Distances (km)
22 Oct	3	110, 125, 98	90, 60	675, 353
23 Oct	2	151, 106	70	445
24 Oct	4	150, 88, 105, 105	30, 60, 75	158, 378, 473
26 Oct	3	*, 115, 110	60, 90	414, 594
27 Oct	4	160, 181, 105, 74	70, 50, 90	760, 315, 400
28 Oct	4	201, 214, 114, 121	60, 55, 50	768, 376, 362
29 Oct	3	93, 117, 141	50, 40	350, 340

[a]The asterisk represents plume initiated within the scanned area and the zonal drifts cannot be resolved from the data set.

[9] Another event on 26 October is presented in Figure 1 (bottom), which show a series of ionograms taken during the period 1125–1245 UT. The first three ionograms show a sequence in which a satellite trace first appears in the third hop (3F) and 10 min later is seen in the first hop (1F). In the third ionogram taken at 1145 UT, multiple (up to 6) satellite traces are seen, which could be associated with the condition that the Digisonde was centered under a crest of LSWS at that time [*Tsunoda*, 2008]. After about 25 min, diffuse spread-F traces (RSF) appeared in the ionogram taken at 1210 UT. From the start of the first satellite trace it took about 45 min for the appearance of RSF. These observations indicate that the satellite traces, indicative of LSWS, appear to be a precursor for the generation of ESF over Sanya, which are similar to those observed at equatorial [e.g., *Lyon et al.*, 1961; *Abdu et al.*, 1981] and other low latitude stations [*Abdu et al.*, 2009b]. Specifically, using conjugate station Digisonde observations, *Abdu et al.* [2009b] observed a tendency for the LSWS to occur simultaneously at low latitude conjugate points and found a time delay in their occurrence of about 20–45 min with respect to the equatorial LSWS. Considering the day-to-day variability of neutral wave dynamics, they suggested that the low latitude LSWS is not likely to result from a magnetically westward propagating neutral disturbance front, but could result from latitudinal extension of the developing bubble 'feet'. If so, the present LSWS events on 24 and 26 October 2011 could be observed at all latitudes equatorward of Sanya in this longitude. More recently, on the basis of TEC measurements from the GRB receivers located at Bac Lieu, Ho Chi Minh City and Nha Trang, *Tulasi Ram et al.* [2012] reported the LSWS, detected at all the three stations, as aligned with magnetic field lines.

[10] Backscatter power profiles obtained from the Sanya VHF radar five-beam steering measurement for the two events of 24 and 26 October are shown in Figures 2a–2e, and Figures 2f–2j, respectively. These are so-called Range-Time-Intensity (RTI) plots, showing the signal-to-noise ratio (SNR, greater than −8 dB) as a function of altitude and UT. The height of the echoes is determined by assuming perpendicularity between the radar beam and the magnetic field line at different range bins using the International Geomagnetic Reference Field (IGRF 2005) model. The azimuth and zenith angles in each direction are shown in the right top of each panel. The variations of scintillation index (S_4) for all GPS satellites are superposed in Figures 2c and 2h (the red dots represent $S_4 > 0.1$). As seen in Figure 2, in general, the radar plumes associated with ESF appeared intermittently with periods varying from 30 to 75 min. The maximum intensity of GPS scintillation coincides well with the strongest ESF echoes during post-sunset hours. The periodic plume structures have also been observed at other equatorial and low latitude stations, for example Gadanki and Kwajalein. Using the FAI observations from the Gadanki MST radar, *Patra and Phanikumar* [2009] reported two cases of periodic irregularity structures commencing respectively at post-sunset and post-midnight hours. *Hysell et al.* [1994] observed many plume structures associated with post-sunset ESF (as large as 11 in number) at Kwajalein. The dominant periodicity observed by them was 30 min. On the basis of the equatorial atmospheric radar (EAR) multibeam observations over Kototabang, *Fukao et al.* [2004] reported that the post-sunset FAIs, with horizontal scales of 50 to 100 km, periodically appear at similar horizontal distances and traverse from west to east. The horizontal distance was quite consistent with the spacing predicted for gravity-wave-seeded plasma upwelling.

[11] In the present analysis, the periodic plume echoes shown in Figure 2 are divided into seven groups. For the event of 24 October, the plumes that occurred around 1230, 1300, 1400, and 1515 UT, are labeled the group 1–4, respectively. For the event of 26 October, the plumes that occurred near 1215, 1315 and 1445 UT, are labeled the group 5–7, respectively. For group 1–4, and 6–7, the plume structures appeared first in the westernmost beam and were seen in all five beams, which mean that their initial appearance must have occurred to the west of the westernmost beam. They drifted eastward into and out of the radar beam following their development at a westward longitude. According to the echo time delay and the horizontal separations (about 300 km) of the easternmost and westernmost beams around 300 km altitude, the zonal drift velocities of plume structures 1–4 and 6–7 are estimated to be approximately 150, 88, 105, 105, 115 and 110 ms^{-1}, respectively. From the drift speeds and the time intervals, the horizontal distance between the adjacent plume groups, are estimated to be about 158, 378, 473, 414 and 594 km, respectively.

[12] Table 2 lists the statistics of horizontal distance for periodic plumes obtained from the Sanya VHF radar five-beam steering measurements. The distances so obtained are comparable with earlier observations of ESF from coherent and incoherent scatter radars, and in situ satellites. It has been proposed that the horizontal distances correspond to the zonal wavelengths of the LSWS. On the basis of multi-instrument observations, *Röttger* [1973], *Singh et al.* [1997] and *Tsunoda* [2005] reported that the ESF irregularity structures, which grew from the upwellings or crests of LSWS, were separated quasiperiodically in longitude by a distance similar to the LSWS wavelength. Results from *Abdu et al.* [2009a] and *Tsunoda et al.* [2011] suggest that the zonal wavelength of LSWS could be controlled by the velocity-shear scale size of the collisional-shear instability [*Hysell and Kudeki*, 2004] and the atmospheric gravity waves (AGW) in the troposphere [e.g., *Tsunoda*, 2005; *Tsunoda et al.*, 2010].

[13] Another feature of interest is the absence or presence of radar plume echoes in the different beams. As is evident from Figures 2f–2j, the first plume (group 5) on 26 October was not detected in the westernmost beam. The closed blue curve highlights this feature which is seen most intense in the easternmost beam. It is also interesting to note that the plume

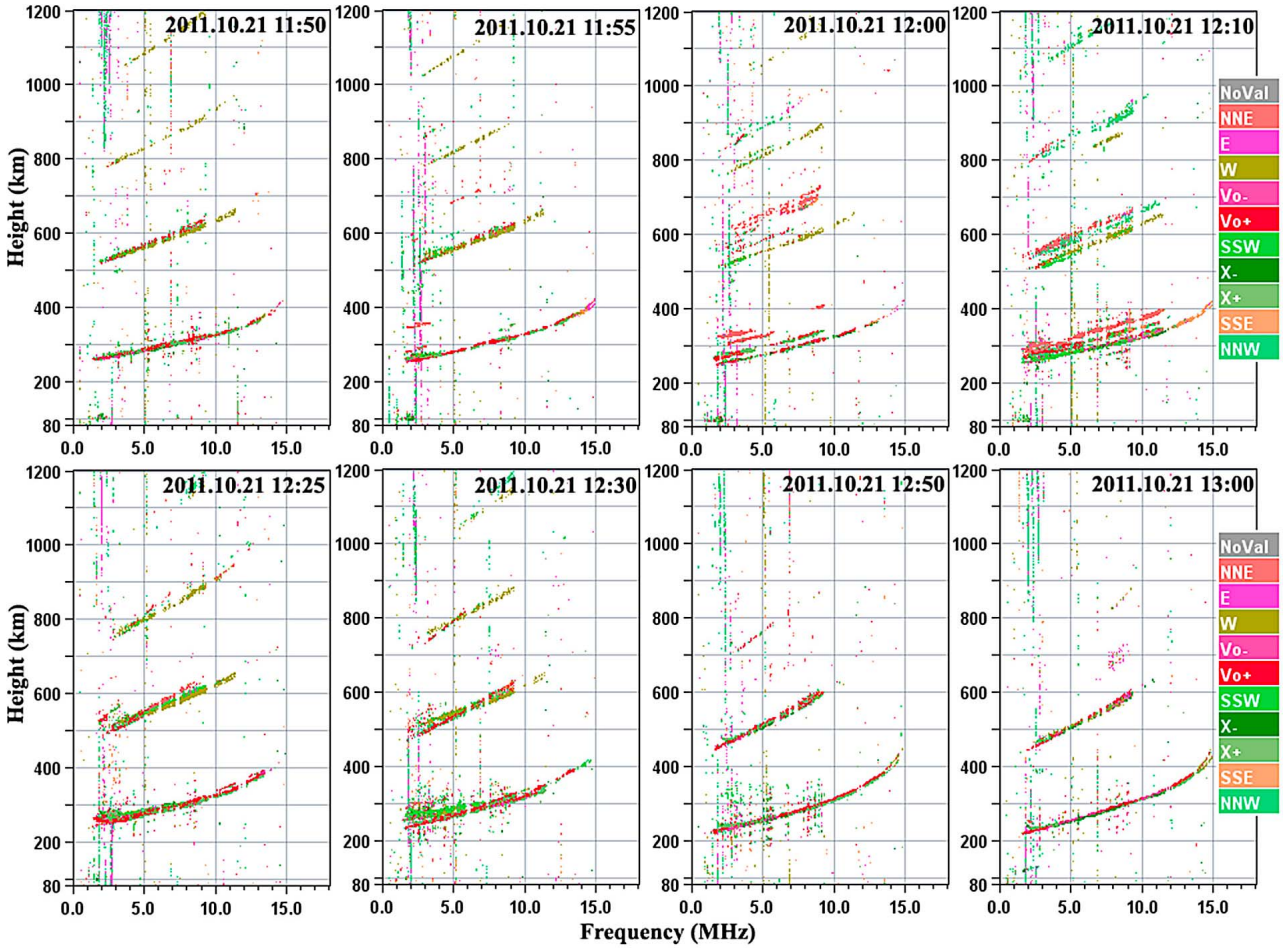

Figure 3. Sequential ionograms taken at 1150–1300 UT on 21 October 2011 over Sanya. The ionograms show that the bottom type spread-F driven by LSWS did not develop vertically and evolve into range type spread-F.

in group 5 detected by the easternmost beam (shown in Figure 2f) initiated at a height of 280 km, and around 1145 UT which corresponds just to apex sunset time. Such a beam-dependent appearance of plumes around sunset is consistent with the observation from radar beam steering measurements at the Pohnpei Radar Observatory (PRO) by *Tsunoda and Ecklund* [2007]. These authors reported that the characteristics of the upwelling bottomside layers varied from beam to beam. A close relationship between the upwelling layers and radar plumes was also found. It was suggested that the modulated upwelling depth and beam dependent plasma plume structure were produced by LSWS. Due to the fact that the field lines at equatorial bottom side F layer map to the E layer over a low latitude location like Sanya, the bottom type layers which usually appear below the plasma plumes at the geomagnetic equator were not observed over Sanya (see Figure 2). Observations from the EAR radar, which is located at similar latitude as Sanya but in the southern hemisphere, also revealed that the bottom type layers are rarely observed [*Fukao et al.*, 2004]. The beam dependent appearance of the plumes, together with the multisatellite traces (up to 6) may indicate that an upwelling or crest of LSWS occurred at sunset hours of 26 October 2011 along the longitudinal sector of Sanya. This provides a consistent evidence that the appearance of LSWS leads to the quite localized generation of ESF plumes after sunset. On the other hand, we note that during the development of post-sunset F region irregularities, the valley region irregularities generation and E region irregularities (ERI) disruption were detected, which are regular phenomena over Sanya during equinoctial months [*Li et al.*, 2011]. Further, we may note that the ERI disruption shown in Figures 2f–2j present a beam dependent behavior, similar to that of plasma plumes around 1200 UT. This could be associated with the mapping of polarization electric field (PEF) generated within the equatorial plasma bubbles (plumes) [e.g., *Patra et al.*, 2005]. The PEF appears to be responsible for the inhibition of the ERI development through the gradient drift instability mechanism, over Sanya.

3.2. Cases of LSWS Without ESF

[14] In the above two cases we described the occurrence characteristics of the ESF and LSWS. The appearance of satellite traces in ionograms and the spatial distribution of plume structures, indicated that the presence of LSWS could be a precursor for the ESF. In this case, we present evidence that the ESF do not always occur while the LSWS is observed near sunset. Figure 3 shows a time sequence of ionograms for

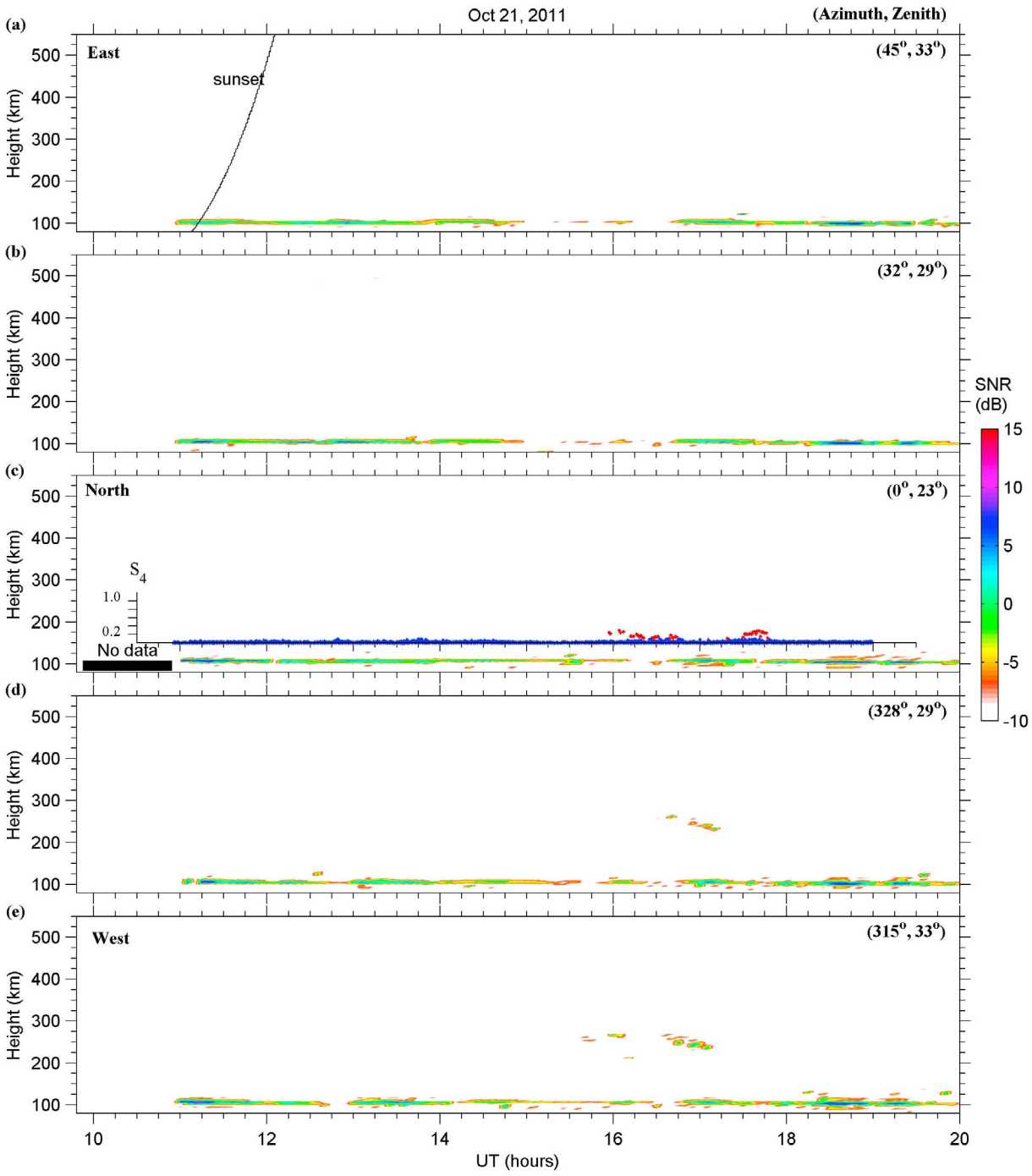

Figure 4. (a–e) RTI maps of backscatter echoes obtained from the Sanya VHF radar five-beam steering measurement on 21 October 2011. The black slant line indicates the sunset time over Sanya. The superimposed dots in Figure 4c show the variations of GPS scintillation index S_4 (red dot means $S_4 > 0.1$). The horizontal bar shows a data gap during 0900–1055 UT due to a power failure.

the evening of 21 October 2011. As can be seen from the first ionogram taken at 1150 UT, no satellite trace was observed. However, just 5 min later, the satellite traces indicative of LSWS were found at 1155 UT in the first hop and continued to exist until 1250 UT with a duration of around 50 min. What appears to be an initiation of a bottom type spread-F (BSF), in the ionogram at 1210 UT, did not evolve further in the subsequent ionograms and by 1250 UT it totally disappeared. This indicates that the BSF did not develop vertically and evolve into post sunset range type spread-F on this evening. Figure 4 shows the RTI map obtained from the radar five-beam steering measurements on the night of 21 October 2011. There is a data gap between 0900 and 1055 UT due to a power failure. As is evident from the RTI plots, no post-sunset plasma plume was detected in all the five beams. The apparent absence of post-sunset GPS

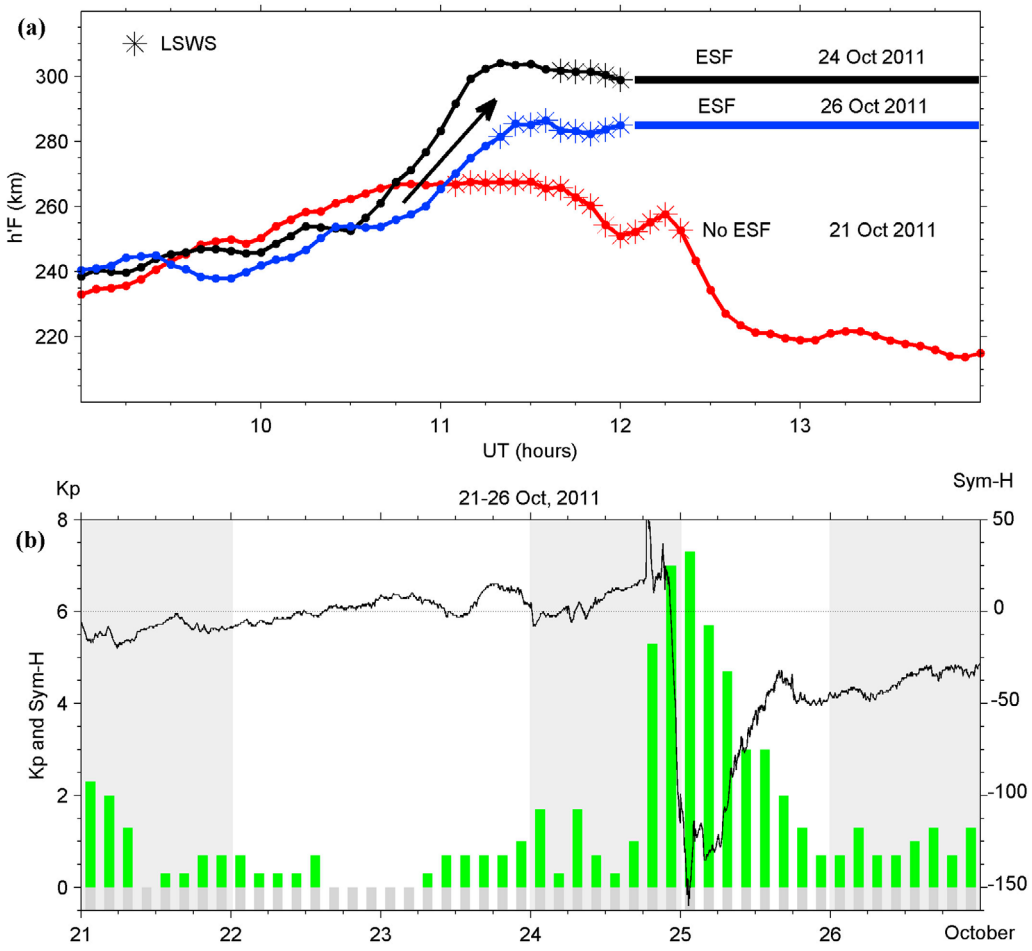

Figure 5. (a) Variations of the minimum virtual height of the F layer (h′F) on 21, 24 and 26 October 2011 over Sanya. The arrow, asterisks and horizontal bars indicate the abrupt increase of sunset F layer on ESF nights, the occurrence of LSWS (satellite traces) and ESF, respectively. (b) The Sym-H and Kp indices on 21–26 October 2011. The shaded areas mark the three days, 21, 24 and 26 October 2011.

scintillation and radar plume development in Figure 4, in contrast to the plumes and scintillation occurrences in Figure 2, indicates that the appearance of LSWS is not a sufficient condition to lead to ESF plume or plasma bubble development. Other factors that are associated with the ambient conditions and dynamic processes in the ionosphere could also play key roles favoring, or inhibiting, the irregularity development [e.g., *Abdu*, 2001]. Using the conjugate point equatorial experiment (COPEX) campaign data in Brazil, *Abdu et al.* [2009b] discussed the importance of the PRE, together with the LSWS and trans-equatorial wind (TEW), in determining the day-to-day variability of ESF.

[15] To investigate the possible dependence of the ESF occurrence on increase in the F layer height when LSWS occurs, we present the variation of the F layer virtual height (h'F) on 21, 24 and 26 October 2011 in Figure 5a. The horizontal bold lines mark the occurrence of ESF. We note that the h'F variation on the non-ESF night (21 October) was obviously different as compared to the h′F variations on both the ESF nights, 24 and 26 October. On the two latter nights the evening h'F values were significantly higher than that on the non ESF night. It is relevant to point out that the variation of h′F over Sanya, which is an off-equatorial site (dip angle 25°) cannot be attributed only to the PRE. Factors such as the meridional winds and diffusion could also play roles in raising or suppressing the height of F layer. Figure 5a shows that an abrupt increase of F layer occurred around 1100 UT (marked by the arrow) on ESF days. The difference in the maximum h′F values between ESF and non-ESF days was about 40 km. A recent study by *Narayanan et al.* [2012] showed that the h′F variations on ESF and non-ESF days were identical in the two cases that they studied. They suggested that the small-scale wave-like structure (SSWS) which they observed on the ESF day was a possible cause for the ESF development. From the present data set, however, we cannot ascertain the presence of SSWS. On the other hand, the apparent connection between the h′F variation and ESF, in terms of the individual events, might call attention to a dependence of ESF on the post-sunset rise of the F layer. This would suggest that the uplift of the evening F layer to enough altitude was an important pre requisite for the generation of the post-sunset ESF, even when the LSWS appeared around sunset. The increase in h′F that produced a corresponding ESF development with topside plumes (Figure 2), though is

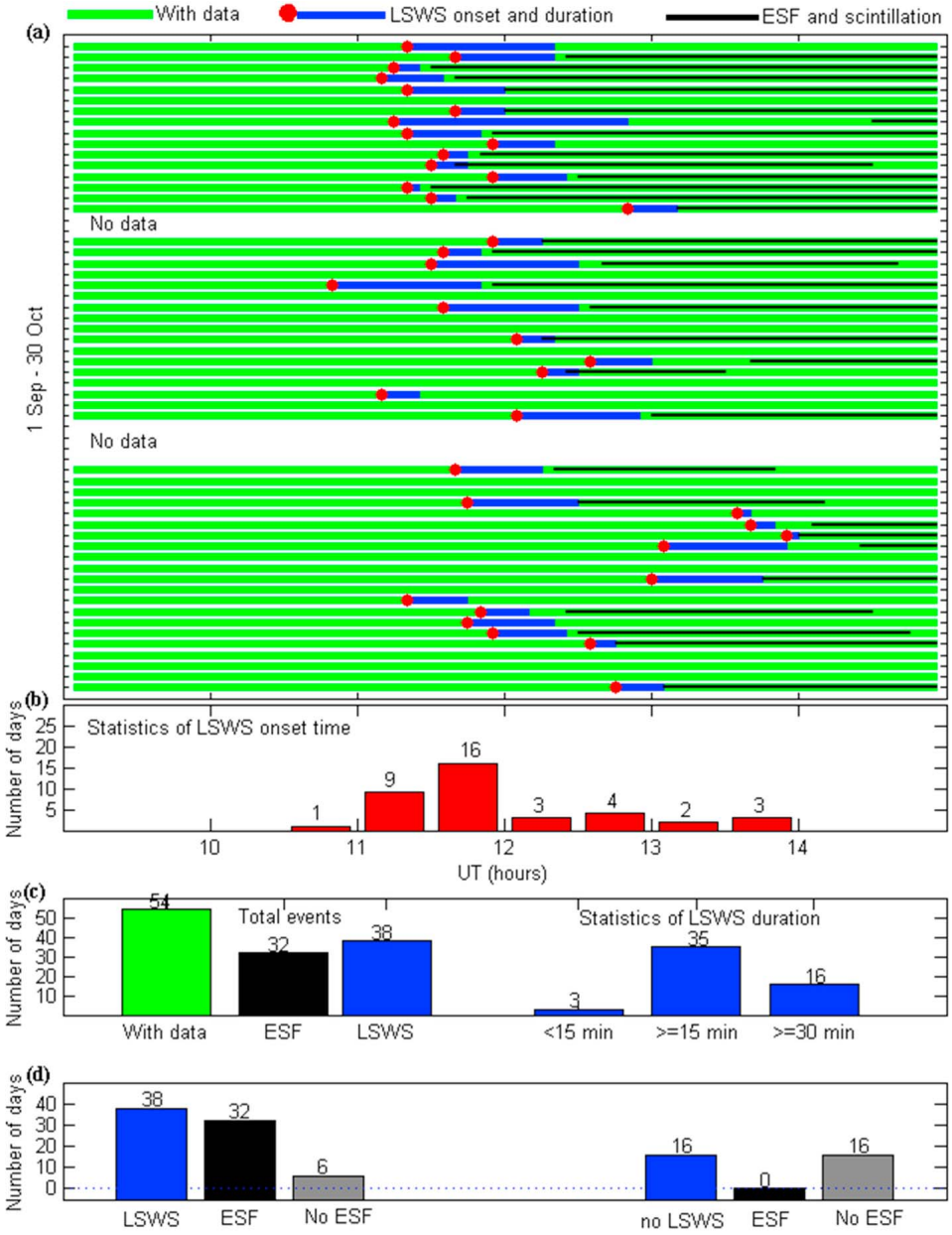

Figure 6. (a) Occurrence of LSWS and ESF producing GPS scintillations during 1 September to 30 October 2011. Also shown are the statistical distribution of LSWS (b) onset time and (c) durations, and (d) the number of days of ESF occurrence or not during LSWS and non-LSWS conditions.

of small magnitude, appears to highlight the role of the PRE in the nonlinear growth of the R-T instability. Height changes downward of such smaller ranges, likely modulated also by the LSWS, may not be in general sufficient to affect the instability nonlinear growth and therefore cause an impact on the generation of bottom type spread F. Figure 5b shows the Sym-H and Kp indices during 21–26 October 2011. It can be noted that on 21 and 26 October 2011, the magnetic activity was quiet (the 3-h Kp value is less than 3). Further, a fairly intense storm started at post-midnight hours, around 1900 UT (LT = UT + 7.5) on 24 October, with a minimum Sym-H (<−150 nT) around 0130 UT on 25 October. As is evident, the sunset h′F difference on the three days, 21, 24 and 26 October, appears unlikely caused by the magnetic disturbance. The day-to-day variability of the PRE and the presence of the LSWS, might have played important roles in the h′F difference observed around the sunset hours [*Tsunoda et al.*, 2010]. Though, the seasonal and solar cycle dependence of the PRE has been well investigated, the day-to-day variability of PRE is still an unresolved problem [e.g., *Fejer et al.*, 1999; *Abdu*, 2001]. Already, *Abdu et al.* [2006] have shown that planetary waves could modulate the PRE strength that could lead to the day-to-day variability of plasma vertical drift near sunset.

3.3. Statistical Dependence of ESF on LSWS and h′F

[16] To examine the dependence of ESF on LSWS, a statistical analysis was performed on the occurrence of the

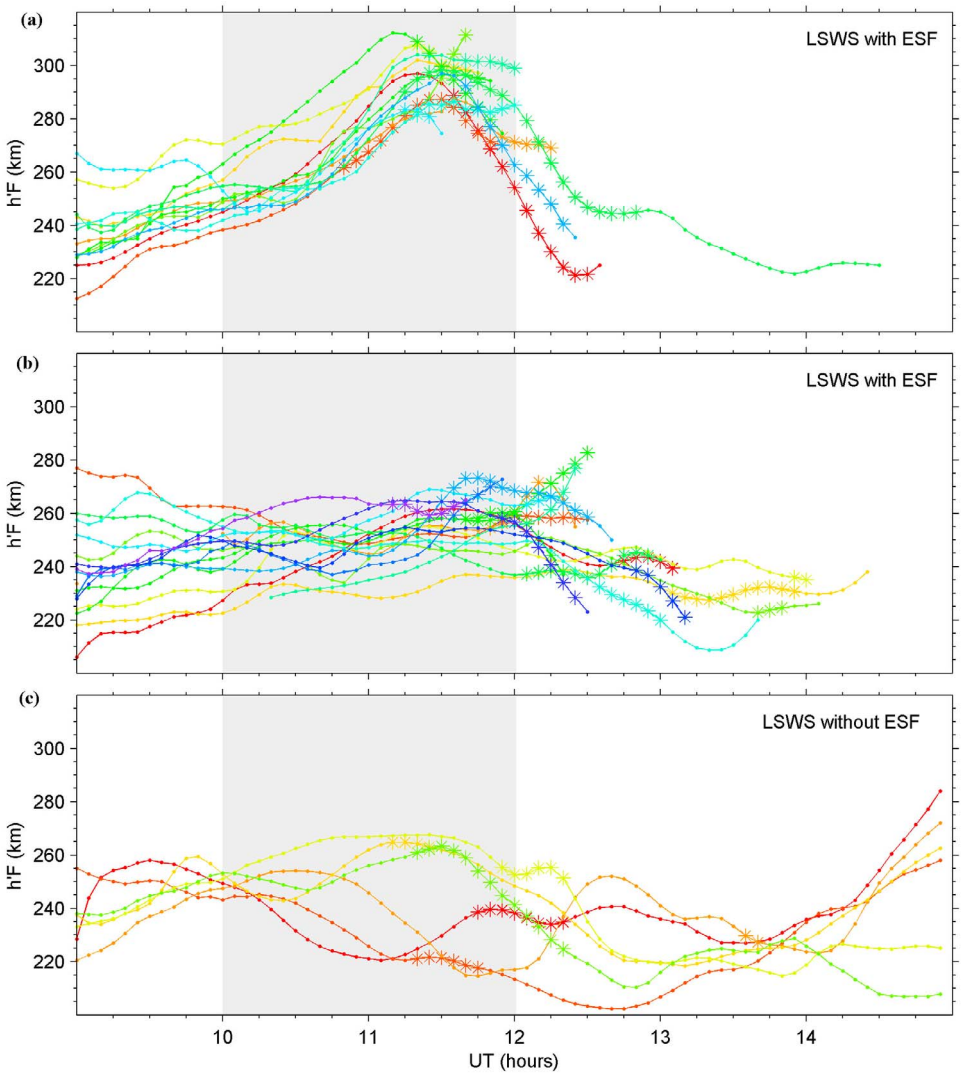

Figure 7. Variations of h′F on (a, b) ESF and (c) non-ESF days during LSWS conditions over Sanya. The asterisk and shaded area show the appearance of LSWS, and the evening hours under the influence of local sunset (LT = UT + 7.5), respectively.

LSWS and the subsequent ESF, and also on the behavior of h′F under the ESF and non-ESF conditions while the LSWS occurs. The results are shown in Figures 6 and 7. Figure 6 presents the statistics of the LSWS onset time and duration, and that of the subsequent post-sunset ESF and GPS scintillation occurrences during 1 September to 30 October 2011. The blue and black bars in Figure 6a show the occurrences of the LSWS and the ESF producing ionospheric scintillations, respectively. The satellite traces onset time is marked by red dot at the beginning of each bar. It can be noted that there is large dispersion in the onset time from one day to another. A statistical analysis on the onset time of the LSWS (Figure 6b) shows that out of 38 events of LSWS, only one event was observed before sunset, around 1035 UT (1800 LT). The generation of post-sunset LSWS was generally thought to be controlled by the collisional-shear instability [*Hysell and Kudeki*, 2004]. However, for the pre-sunset LSWS, a possibility of loading of the *F* region dynamo by a sunlit E region was proposed by *Tsunoda et al.* [2011]. From the GRBR TEC measurements over Vietnam, the authors reported that the seeds for LSWS could appear in the late afternoon and the amplification could take place mostly during the PRE. This suggests that during the initial phase of the LSWS, the seed amplitude may be not large enough to be detected by Digisonde, in the form of 'satellite traces' in ionograms. Thus, the onset time of the 'satellite traces' shown in Figure 6b could be somewhat later than that of the LSWS. Figure 6c shows the total number of the ESF and LSWS and the statistics of the duration of the later. The left three bars in this panel show that there are 54 nights with simultaneous ionogram, VHF radar and scintillation data during the period, of which the numbers of days with LSWS and ESF responsible for scintillation occurrence are 38 and 32, respectively. As is evident from the right three bars in Figure 6c, most LSWS events continued to exist for more than 15 min in ionograms. Out of the 38 events of the LSWS, 3 have been observed with

durations less than 15 min. Figure 6d shows the number distribution of the ESF and no ESF nights for both the LSWS and no LSWS cases. Out of the 38 events of LSWS, 32 events lead to ESF development. There are 6 events of LSWS without subsequent evolution of ESF. This statistical result adds additional evidence in support of the suggestion by *Narayanan et al.* [2012] that the presence of LSWS alone is not sufficient to trigger the development of ESF. On the other hand, we note that all the ESF events were preceded by the occurrence of LSWS, consistent with previous observations on satellite traces and subsequent ESF development. Using ionograms taken at Fortaleza with a time resolution of 15 min, *Abdu et al.* [1981] reported that satellite traces preceded occurrences of ESF on all but two nights. However, the absence of satellite traces on ESF days shown by the authors may not indicate the absence of LSWS, since as revealed by Figure 6d there are 3 events of LSWS with durations less than 15 min. Therefore, exceptional cases that ESF occurred without satellite traces could be associated with the longer time intervals between the ionograms.

[17] Figure 7 presents the variation of the h′F for all the LSWS events during 0900–1500 UT. We divided the database into two categories: one of ESF occurrence (Figures 7a and 7b) and the other of nonoccurrence (Figure 7c). Further, Figures 7a and 7b present the h′F variations with and without post-sunset rise (an uplift of F layer more than 45 km near sunset) on ESF days, respectively. As can be seen from Figure 7a, the individual ESF events are preceded by substantial post-sunset rise of the F layer, indicating significant vertical drift as well. The F-layer uplift, in association with the presence of LSWS, provides favorable conditions for the initiation and growth of the Rayleigh-Taylor instability. This result reveals that the LSWS and ESF have nearly a one-to-one relationship, which is consistent with recent case studies. On the other hand, Figure 7b shows the occurrence of ESF producing ionospheric scintillations even when the uplift of the F layer was not observed around sunset. The absence of the any post-sunset layer rise may indicate that the LSWS that appeared over Sanya longitude led to the generation of the ESF, and therefore in this case the ESF appears more closely related to LSWS than to the PRE. In Figure 7c, the F layer altitude variation was comparable to that shown in Figure 7b, however, no ESF and GPS scintillation was observed during the hours following the LSWS occurrence. Though many case studies have shown that the precursor density perturbations (needed to initiate the plasma instability) in the form of LSWS always precede the occurrence of ESF, the absence of ESF in Figure 7c, in contrast to the ESF development in Figures 7a and 7b, is further evidence that under weak or inexpressive PRE conditions, the appearance of LSWS alone may not be sufficient for the ESF development. In fact the result in Figure 7c clearly suggests that under low F layer heights ($<\sim$260 km in this case) near sunset, marked by the almost total absence of the PRE, the mere presence of LSWS does not lead to any ESF development. In this context it will be interesting to verify if other factors, such as the appearance of small-scale wave-like structures reported by *Narayanan et al.* [2012], could play any role favoring the generation of ESF. Another factor that appears to merit consideration is the possible role of a meridional (poleward) wind that could have suppressed the PRE vertical drift and post sunset F layer height over Sanya, at the same time suppressing the ESF instability nonlinear growth [e.g., *Maruyama*, 1988; *Abdu et al.*, 2009b].

4. Summary and Conclusions

[18] The occurrence statistics of ESF and LSWS have been obtained from the Sanya VHF radar, Digisonde and GPS scintillation data taken during the period 1 September to 30 October 2011. We analyzed the onset time and duration distribution of the LSWS, identified as satellites traces in the ionogram records. The evolution characteristics of plume structures obtained from the radar five-beam steering measurements, and from the dependence of the ESF and scintillation on the LSWS were investigated. The main results and conclusion from this study may be summarized as follows.

[19] 1. All the ESF events observed were preceded by LSWS, suggesting that the perturbations that must have originated near the base of the F layer at equatorial latitude had reached the base of the F layer at Sanya latitude in this longitude. A statistics on the duration of LSWS shows that out of 38 LSWS events, there are 3 events with durations less than 15 min. Earlier observations on the occurrence of ESF without LSWS (satellite trace) could be associated with the long time interval between ionograms. This result thus reveals that LSWS is a necessary precursor signature for the generation of equatorial F region irregularities producing ionospheric scintillation. From the absence of LSWS around sunset, one may infer the nonoccurrence of ESF during following hours.

[20] 2. The LSWS and ESF nearly had a one-to-one relationship when the sunset F layer was lifted, obviously. That is, the concurrence of the LSWS and the evening vertical drifts (large enough) may provide the necessary and sufficient conditions for the ESF development. However, in the absence of the post-sunset rise (or weak increase) in the F layer height, the appearance of the LSWS alone may not be sufficient for the ESF development.

[21] 3. The LSWS was not always followed by the ESF development. Out of 38 events of LSWS, there are 6 events without subsequent evolution of ESF. This provides statistically consistent evidence corroborating the recent case study result by *Narayanan et al.* [2012] and appears to strengthen the suggestion that neither the LSWS nor the post-sunset rise of the F layer is alone sufficient to cause the development of ESF. On the other hand, when a weak or negative PRE may not lead to nonlinear growth of plasma instability responsible for ESF growth it may not have an impact sufficient enough to suppress the generation of bottom type spread F that may be driven by LSWS.

[22] 4. The spatial distribution of the periodic plumes as obtained by the Sanya VHF radar five-beam steering measurements appears to reveal an inter-plume separation that varies from 150 to 770 km, which agrees with the earlier wavelength measurements of the LSWS. The beam dependent appearance of the plume structures, which were initiated within the scanned area and were not detected in the westernmost beam, shows that the five-beam steering measurements of Sanya VHF radar could be well used to investigate the quite localized generation of ESF plumes over Sanya longitude.

[23] The results of present investigation may pose an important question as to what implications these may have

for the factors controlling the storm time ESF development that have been observed to extend in extremely narrow or wide longitudinal ranges [e.g., *Li et al.*, 2010]. There is a clear need to understand the longitudinal distribution of LSWS. Further, more beam-steering measurements from the Sanya VHF radar will be carried out in the season of high ESF occurrence (equinoctial months March–April and September–October), which will help to investigate the day-to-day variability of ESF seeded by LSWS.

[24] **Acknowledgments.** This research is supported by the Natural Science Foundation of China (40904038, 41074113, 41174136 and 41004072), Chinese Academy of Sciences (KZCX2-YW-Y10, KZZD-EW-01-2, KZZD-EW-01-3) and National Important Basic Research Project of China (2011CB811405). The Sym-H and Kp data were obtained from World Data Center for Geomagnetism, Kyoto.

[25] Robert Lysak thanks the reviewers for their assistance in evaluating the paper.

References

Abdu, M. A. (2001), Outstanding problems in the equatorial ionosphere thermosphere electrodynamics relevant to spread F, *J. Atmos. Sol. Terr. Phys.*, *63*, 869–884, doi:10.1016/S1364-6826(00)00201-7.

Abdu, M. A., I. S. Batista, and J. A. Bittencourt (1981), Some characteristics of spread F at the magnetic equatorial station Fortaleza, *J. Geophys. Res.*, *86*(A8), 6836–6842, doi:10.1029/JA086iA08p06836.

Abdu, M. A., R. T. de Medeiros, J. A. Bittencourt, and I. S. Batista (1983), Vertical ionization drift velocities and range type spread F in the evening equatorial ionosphere, *J. Geophys. Res.*, *88*(A1), 399–402, doi:10.1029/JA088iA01p00399.

Abdu, M. A., P. P. Batista, I. S. Batista, C. G. M. Brum, A. J. Carrasco, and B. W. Reinisch (2006), Planetary wave oscillations in mesospheric winds, equatorial evening prereversal electric field and spread F, *Geophys. Res. Lett.*, *33*, L07107, doi:10.1029/2005GL024837.

Abdu, M. A., E. Alam Kherani, I. S. Batista, E. R. de Paula, D. C. Fritts, and J. H. A. Sobral (2009a), Gravity wave initiation of equatorial spread F/plasma bubble irregularities based on observational data from the SpreadFEx campaign, *Ann. Geophys.*, *27*, 2607–2622, doi:10.5194/angeo-27-2607-2009.

Abdu, M. A., I. S. Batista, B. W. Reinisch, J. R. de Souza, J. H. A. Sobral, T. R. Pedersen, A. F. Medeiros, N. J. Schuch, E. R. de Paula, and K. M. Groves (2009b), Conjugate Point Equatorial Experiment (COPEX) campaign in Brazil: Electrodynamics highlights on spread *F* development conditions and day-to-day variability, *J. Geophys. Res.*, *114*, A04308, doi:10.1029/2008JA013749.

Chapagain, N. P., B. G. Fejer, and J. L. Chau (2009), Climatology of postsunset equatorial spread *F* over Jicamarca, *J. Geophys. Res.*, *114*, A07307, doi:10.1029/2008JA013911.

Fejer, B. G., L. Scherliess, and E. R. de Paula (1999), Effects of the vertical plasma drift velocity on the generation and evolution of equatorial spread *F*, *J. Geophys. Res.*, *104*(A9), 19,859–19,869, doi:10.1029/1999JA900271.

Fukao, S., Y. Ozawa, T. Yokoyama, M. Yamamoto, and R. T. Tsunoda (2004), First observations of the spatial structure of *F* region 3-m-scale field-aligned irregularities with the Equatorial Atmosphere Radar in Indonesia, *J. Geophys. Res.*, *109*, A02304, doi:10.1029/2003JA010096.

Huba, J. D., G. Joyce, and J. Krall (2008), Three-dimensional equatorial spread *F* modeling, *Geophys. Res. Lett.*, *35*, L10102, doi:10.1029/2008GL033509.

Hysell, D. L., and J. Burcham (2002), Long term studies of equatorial spread F using the JULIA radar at Jicamarca, *J. Atmos. Sol. Terr. Phys.*, *64*, 1531–1543, doi:10.1016/S1364-6826(02)00091-3.

Hysell, D. L., and E. Kudeki (2004), Collisional shear instability in the equatorial *F* region ionosphere, *J. Geophys. Res.*, *109*, A11301, doi:10.1029/2004JA010636.

Hysell, D. L., M. C. Kelley, W. E. Swartz, and D. T. Farley (1994), VHF radar and rocket observations of equatorial spread *F* on Kwajalein, *J. Geophys. Res.*, *99*(A8), 15,065–15,085, doi:10.1029/94JA00476.

Kil, H., and R. A. Heelis (1998), Global distribution of density irregularities in the equatorial ionosphere, *J. Geophys. Res.*, *103*(A1), 407–417, doi:10.1029/97JA02698.

Li, G., B. Ning, L. Liu, Z. Ren, J. Lei, and S.-Y. Su (2007), The correlation of longitudinal/seasonal variations of evening equatorial pre-reversal drift and of plasma bubbles, *Ann. Geophys.*, *25*, 2571–2578, doi:10.5194/angeo-25-2571-2007.

Li, G., et al. (2010), Longitudinal development of low-latitude ionospheric irregularities during the geomagnetic storms of July 2004, *J. Geophys. Res.*, *115*, A04304, doi:10.1029/2009JA014830.

Li, G., B. Ning, A. K. Patra, W. Wan, and L. Hu (2011), Investigation of low-latitude *E* and valley region irregularities: Their relationship to equatorial plasma bubble bifurcation, *J. Geophys. Res.*, *116*, A11319, doi:10.1029/2011JA016895.

Lyon, A. J., N. J. Skinner, and R. W. Wright (1961), Equatorial spread F at Ibadan, Nigeria, *J. Atmos. Terr. Phys.*, *21*, 100–119, doi:10.1016/0021-9169(61)90104-0.

Maruyama, T. (1988), A diagnostic model for equatorial spread F: 1. Model description and application to electric field and neutral wind effects, *J. Geophys. Res.*, *93*(A12), 14,611–14,622, doi:10.1029/JA093iA12p14611.

Narayanan, V. L., A. Taori, A. K. Patra, K. Emperumal, and S. Gurubaran (2012), On the importance of wave-like structures in the occurrence of equatorial plasma bubbles: A case study, *J. Geophys. Res.*, *117*, A01306, doi:10.1029/2011JA017054.

Patra, A. K., and D. V. Phanikumar (2009), Intriguing aspects of *F* region plasma irregularities revealed by the Gadanki radar observations during the SAFAR campaign, *Ann. Geophys.*, *27*, 3781–3790, doi:10.5194/angeo-27-3781-2009.

Patra, A. K., T. Yokoyama, M. Yamamoto, S. Saito, T. Maruyama, and S. Fukao (2005), Disruption of E region echoes observed by the EAR during the development phase of equatorial spread F: A manifestation of electrostatic field coupling, *Geophys. Res. Lett.*, *32*, L17104, doi:10.1029/2005GL022868.

Retterer, J. M. (2010), Forecasting low-latitude radio scintillation with 3-D ionospheric plume models: 1. Plume model, *J. Geophys. Res.*, *115*, A03306, doi:10.1029/2008JA013839.

Röttger, J. (1973), Wave-like structures of large-scale equatorial spread-*F* irregularities, *J. Atmos. Terr. Phys.*, *35*, 1195–1206, doi:10.1016/0021-9169(73)90016-0.

Singh, S., F. S. Johnson, and R. A. Power (1997), Gravity wave seeding of equatorial plasma bubbles, *J. Geophys. Res.*, *102*(A4), 7399–7410, doi:10.1029/96JA03998.

Takahashi, H., et al. (2009), Simultaneous observation of ionospheric plasma bubbles and mesospheric gravity waves during the SpreadFEx Campaign, *Ann. Geophys.*, *27*, 1477–1487, doi:10.5194/angeo-27-1477-2009.

Thampi, S. V., M. Yamamoto, R. T. Tsunoda, Y. Otsuka, T. Tsugawa, J. Uemoto, and M. Ishii (2009), First observations of large-scale wave structure and equatorial spread F using CERTO radio beacon on the C/NOFS satellite, *Geophys. Res. Lett.*, *36*, L18111, doi:10.1029/2009GL039887.

Tsunoda, R. T. (2005), On the enigma of day-to-day variability in equatorial spread *F*, *Geophys. Res. Lett.*, *32*, L08103, doi:10.1029/2005GL022512.

Tsunoda, R. T. (2006), Day-to-day variability in equatorial spread *F*: Is there some physics missing?, *Geophys. Res. Lett.*, *33*, L16106, doi:10.1029/2006GL025956.

Tsunoda, R. T. (2008), Satellite traces: An ionogram signature for large-scale wave structure and a precursor for equatorial spread *F*, *Geophys. Res. Lett.*, *35*, L20110, doi:10.1029/2008GL035706.

Tsunoda, R. T., and W. L. Ecklund (2007), On the post-sunset rise of the equatorial *F* layer and superposed upwellings and bubbles, *Geophys. Res. Lett.*, *34*, L04101, doi:10.1029/2006GL028832.

Tsunoda, R. T., D. M. Bubenik, S. V. Thampi, and M. Yamamoto (2010), On large-scale wave structure and equatorial spread *F* without a post-sunset rise of the *F* layer, *Geophys. Res. Lett.*, *37*, L07105, doi:10.1029/2009GL042357.

Tsunoda, R. T., M. Yamamoto, T. Tsugawa, T. L. Hoang, S. Tulasi Ram, S. V. Thampi, H. D. Chau, and T. Nagatsuma (2011), On seeding, large-scale wave structure, equatorial spread *F*, and scintillations over Vietnam, *Geophys. Res. Lett.*, *38*, L20102, doi:10.1029/2011GL049173.

Tulasi Ram, S., M. Yamamoto, R. T. Tsunoda, S. V. Thampi, and S. Gurubaran (2012), On the application of differential phase measurements to study the zonal large scale wave structure (LSWS) in the ionospheric electron content, *Radio Sci.*, *47*, RS2001, doi:10.1029/2011RS004870.